

# Non-Thermal Emission From IC1262, a Low Temperature Galaxy Cluster

Daniel S. Hudson,<sup>1</sup> Mark Henriksen,<sup>1</sup> and Sergio Colafrancesco<sup>2</sup>

<sup>1</sup> *Joint Center for Astrophysics, University of Maryland Baltimore County*

<sup>2</sup> *Osservatorio Astronomico di Roma*

We report an analysis of IC1262, the lowest temperature galaxy cluster known to have a diffuse nonthermal component in both the radio and X-ray. The diffuse nonthermal X-ray component is detected above the thermal spectrum in the BeppoSAX Medium Energy Concentrator spectrometer detector. A temperature map produced from the Chandra data shows evidence of shock heating in the intracluster medium, and a smoothed flux image contains an asymmetric surface brightness feature aligned with the diffuse radio emission. Diffuse nonthermal emission in massive clusters (e.g., Coma, Abell 754, Abell 2256) is thought to be due to cosmic rays accelerated at shock fronts produced in major mergers. We conclude that these data indicate that even a low mass system, such as IC1262, can experience a significant merger that will produce cosmic-ray acceleration at the shock front.

## 1. Introduction

Recent Chandra observations indicate that relativistic plasma injected into the intracluster medium (ICM) from radio sources eventually detaches from the radio source, forming bubbles of radio plasma in the ICM (McNamara et al. 2001; Heinz et al. 2002; Fabian et al. 2003). In the model proposed by Enßlin (1999), these radio ghosts survive in the ICM, and provide a seed population of Cosmic Rays (CRs). Diffuse non-thermal (NT) emission is produced when merger induced shocks reaccelerate, via the first order Fermi process, this seed CR population. Current evidence suggests that these radio ghosts contain a significant population of protons as well as electrons (Enßlin 1999). Since Blasi (2001) demonstrated that diffuse NT X-ray emission could be produced by either primary electrons directly accelerated at shock fronts, or secondary electrons produced during proton-proton collisions, there are two possible sources for the observed diffuse NT emission. To determine the mechanism that produces diffuse NT emission requires accurate measurement of the spectrum and location of the NT emission.

Simulations by Miniati et al. (2001) show that diffuse NT emission occurs in a broad mass range of clusters with a luminosity proportional to the X-ray temperature, making cool clusters and groups an important diagnostic for understanding which population of electrons produces diffuse NT emission. They find that spectral index of the diffuse NT emission is dependent on the electron population producing the emission, such that the spectral index of diffuse NT emission produced from primary electrons has a steep spectral index ( $\alpha_{ic} > 1.1$ ) while for secondary it is systematically flatter ( $\alpha_{ic} < 1.1$ ).

Hudson et al. (2003) reported detection of diffuse NT emission X-ray and radio emission from IC1262, a poor cluster of galaxies, using the *BeppoSAX* MECS detector. Although the MECS was able to constrain the region of the NT emission, it does not have the spatial resolution to identify the source of the NT emission. In this paper,

we show that the *Chandra* Advanced CCD Imaging Spectrometer (ACIS) has the energy range and spatial capability to detect, localize, and characterize the spectrum of NT X-ray emission from low temperature clusters. These results are compared to simulations of cosmic-ray acceleration at shock fronts produced by cluster merger.

## 2. Observations and Methods

The IC1262 galaxy cluster is a poor cluster of galaxies located at (J2000)  $17^h 33^m 01.0^s$ ,  $+43^\circ 45' 28''$  (Ebeling et al. 1998) with a redshift of 0.0343 (Colles et al. 1999), so that  $1' = 46 h_{65}^{-1}$  kpc. It was observed by the *Chandra* ACIS S3 chip on 23 August 2001 for  $\sim 31$  ksec. The total count rate of the uncleaned data is  $10.2 \pm 0.02$  cts  $s^{-1}$  with peak of  $37 \pm 3$  cts  $s^{-1}$ , which is well below the saturation limit of the ACIS chips operating in Faint Mode ( $170$  cts  $s^{-1}$ ). Figure 1 is a color coded intensity map that shows the full  $8'.5 \times 8'.5$  image in the 0.3–8.0 keV band. The image was obtained using processing routines outlined in the CIAO 2.3 Science Threads<sup>1</sup>. The data was CTI corrected and cleaned for flares, point sources and anomalous high background. Exposure maps were created for 17 different energy bands to ensure proper exposure correction. Background was taken from the CALDB 2.21 blank-sky datasets.

## 3. Results and Analysis

From the flux and hardness maps, Figure 1 and Figure 2 respectively, we chose four regions that have strong gradients in flux and hardness. These regions are shown in Figure 1. We considered four models of background subtraction, to ensure that any NT detection would not be the result of undersubtracted particle background. These four background subtraction techniques were: (1) standard blank-sky fields extracted from the same region on the S3 Chip as the source and normalizing in

<sup>1</sup> <http://cxc.harvard.edu/ciao/threads/index.html>

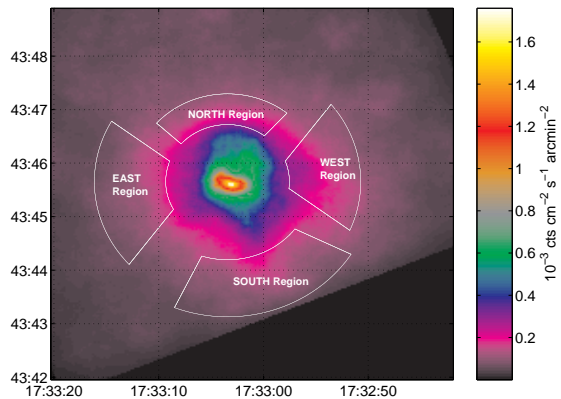


FIG. 1.— Chandra Exposure and CTI Corrected, Background Subtracted Flux Map of IC1262. The white figures are regions extracted to search for possible non-thermal emission.

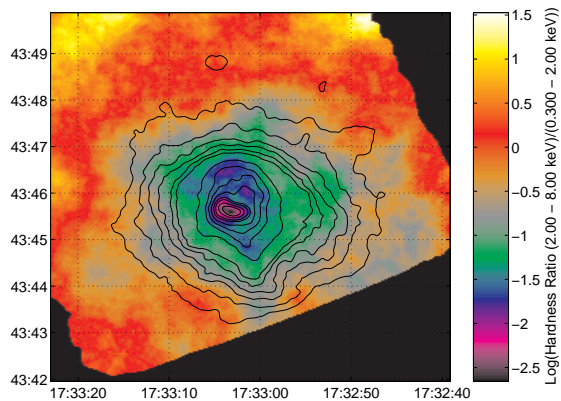


FIG. 2.— Log scale Hardness Map of IC1262 including the 4 regions compact isophote regions.  $(2.0\text{--}8.0\text{ keV})/(0.3\text{--}2.0\text{ keV})$

the 10–12 keV range as described in Markevitch et al. (2003), (2) extracting a region far to the North of the peak flux, modeling it and then using the model times a free constant in our source + background spectrum modeling, (3) freezing the background model described in (2) with a constant proportional to the difference in size of the source and background region, and (4) subtracting the size-normalized background spectrum from the source spectrum. In all cases the source model parameters are consistent within 90% confidence, indicating that all four methods produce the same results.

We modeled our four “possible shock” regions with a single thermal component model, a double component thermal model, and a thermal model with power-law. The addition of the power-law component does not significantly improve the fit in the Eastern and Western regions. In addition, Figure 4 shows that a thermal model fits the entire spectrum in the Eastern Region. In the case of the Northern region, adding either a second thermal component, or a power-law component improves the fit. The single thermal model fit to the Southern region has clear high end residuals (see Figure 4). Adding a second thermal component produces an unconstrained high temperature, however adding a power-law component improves the fit and reduces the residuals (see Figure 4). In order to confirm that this detection was not simply un-

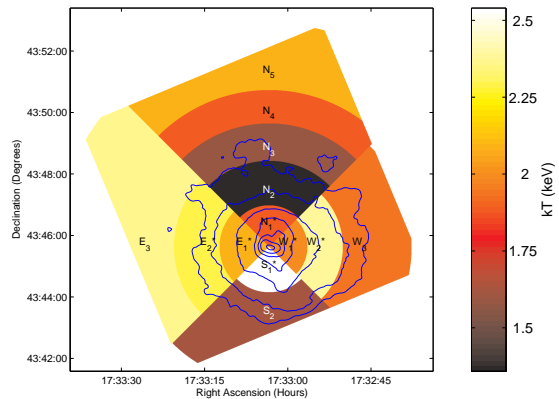


FIG. 3.— Temperature Map of IC1262. Regions with a (\*) have Temperatures given for the double thermal model.

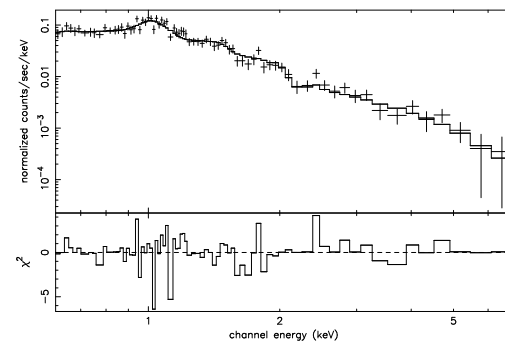
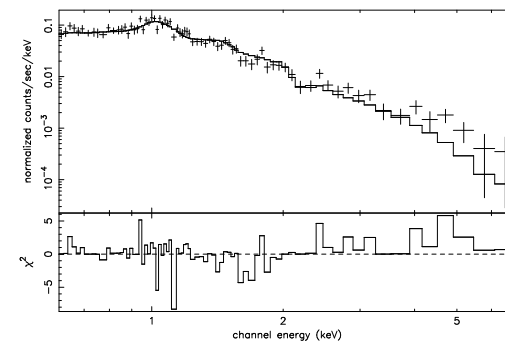
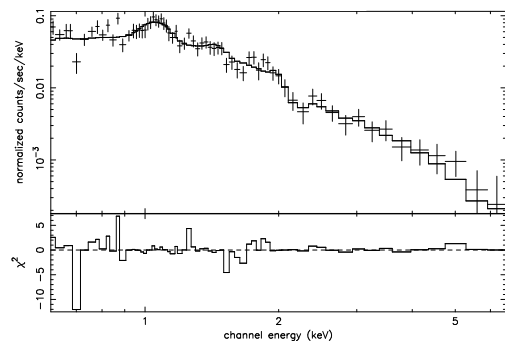


FIG. 4.— Spectral fits to regions of compact isophotes: top is single thermal fit to Eastern Region, middle is single thermal fit to Southern Region, and bottom is thermal + power-law fit to the Southern Region.

TABLE 1. SPECTRAL FITS OF REGIONS.

Region	Model <sup>†</sup>	kT <sub>1</sub> (keV)	Abundance	kT <sub>2</sub> (keV)	χ <sup>2</sup> /dof
N <sub>1</sub>	Apec	1.27 <sup>+0.03</sup> <sub>-0.03</sub>	0.14 <sup>+0.03</sup> <sub>-0.03</sub>		173.0422/98
N <sub>1</sub>	Apec+Apec	1.88 <sup>+0.17</sup> <sub>-0.15</sub>	0.44 <sup>+0.17</sup> <sub>-0.14</sub>	0.83 <sup>+0.16</sup> <sub>-0.04</sub>	134.0729/96
N <sub>2</sub>	Apec	1.34 <sup>+0.12</sup> <sub>-0.04</sub>	0.14 <sup>+0.05</sup> <sub>-0.03</sub>		119.7284/91
N <sub>3</sub>	Apec	1.57 <sup>+0.13</sup> <sub>-0.16</sub>	0.12 <sup>+0.07</sup> <sub>-0.05</sub>		57.09452/76
N <sub>4</sub>	Apec	1.88 <sup>+0.43</sup> <sub>-0.37</sub>	0.13 <sup>+0.14</sup> <sub>-0.08</sub>		65.19046/59
N <sub>5</sub>	Apec	2.09 <sup>+0.95</sup> <sub>-0.58</sub>	0.12 <sup>+0.34</sup> <sub>-0.12</sub>		55.56707/48
W <sub>1</sub>	Apec	1.80 <sup>+0.09</sup> <sub>-0.12</sub>	0.25 <sup>+0.06</sup> <sub>-0.05</sub>		126.3223/108
W <sub>1</sub>	Apec+Apec	1.98 <sup>+0.12</sup> <sub>-0.13</sub>	0.38 <sup>+0.11</sup> <sub>-0.09</sub>	0.61 <sup>+0.20</sup> <sub>-0.24</sub>	113.5917/106
W <sub>2</sub>	Apec	2.09 <sup>+0.18</sup> <sub>-0.12</sub>	0.33 <sup>+0.11</sup> <sub>-0.08</sub>		136.9889/101
W <sub>2</sub>	Apec+Apec	2.38 <sup>+0.22</sup> <sub>-0.21</sub>	0.57 <sup>+0.25</sup> <sub>-0.16</sub>	0.28 <sup>+0.09</sup> <sub>-0.08</sub>	123.7163/99
W <sub>3</sub>	Apec	1.93 <sup>+0.16</sup> <sub>-0.16</sub>	0.18 <sup>+0.07</sup> <sub>-0.06</sub>		118.0369/107
S <sub>1</sub>	Apec	1.62 <sup>+0.05</sup> <sub>-0.05</sub>	0.27 <sup>+0.05</sup> <sub>-0.04</sub>		203.8204/103
S <sub>1</sub>	Apec+Apec	2.54 <sup>+0.26</sup> <sub>-0.22</sub>	0.63 <sup>+0.13</sup> <sub>-0.22</sub>	1.05 <sup>+0.21</sup> <sub>-0.07</sub>	147.7749/101
S <sub>2</sub>	Apec	1.60 <sup>+0.08</sup> <sub>-0.10</sub>	0.17 <sup>+0.06</sup> <sub>-0.05</sub>		134.1819/97
E <sub>1</sub>	Apec	1.62 <sup>+0.05</sup> <sub>-0.06</sub>	0.22 <sup>+0.05</sup> <sub>-0.04</sub>		114.6884/101
E <sub>1</sub>	Apec+Apec	2.08 <sup>+0.32</sup> <sub>-0.16</sub>	0.49 <sup>+0.28</sup> <sub>-0.13</sub>	0.82 <sup>+0.21</sup> <sub>-0.08</sub>	87.91611/99
E <sub>2</sub>	Apec	2.02 <sup>+0.21</sup> <sub>-0.18</sub>	0.23 <sup>+0.11</sup> <sub>-0.08</sub>		90.03336/89
E <sub>2</sub>	Apec+Apec	2.30 <sup>+0.29</sup> <sub>-0.36</sub>	0.40 <sup>+0.23</sup> <sub>-0.20</sub>	0.23 <sup>+0.09</sup> <sub>-0.21</sub>	83.43614/87
E <sub>3</sub>	Apec	2.37 <sup>+0.37</sup> <sub>-0.37</sub>	0.39 <sup>+0.25</sup> <sub>-0.17</sub>		109.8093/99

<sup>†</sup>All models include photoelectric absorption using Wisconsin cross-sections

TABLE 2. NON-THERMAL DETECTION IN THE NORTH AND SOUTH REGIONS.

Region	Background Model	kT <sub>1</sub> (keV)	Abundance	Γ <sub>X</sub>	Non-thermal Normalization(×10 <sup>-4</sup> )	χ <sup>2</sup> /dof
North	blank-sky	1.32 <sup>+0.15</sup> <sub>-0.12</sub>	> 1.00 <sup>+&gt;0.0</sup> <sub>-0.79</sub>	2.36 <sup>+0.14</sup> <sub>-0.12</sub>	0.79 <sup>+0.09</sup> <sub>-0.34</sub>	52.93678/50
	model-bkg	1.29 <sup>+0.16</sup> <sub>-0.13</sub>	> 1.00 <sup>+&gt;0.0</sup> <sub>-0.73</sub>	2.30 <sup>+0.19</sup> <sub>-0.17</sub>	0.78 <sup>+0.11</sup> <sub>-0.35</sub>	54.05200/49
	model-bkg(Frzn)	1.31 <sup>+0.17</sup> <sub>-0.14</sub>	0.39 <sup>+&gt;0.61</sup> <sub>-0.15</sub>	2.41 <sup>+0.24</sup> <sub>-0.45</sub>	0.56 <sup>+0.22</sup> <sub>-0.35</sub>	57.22508/50
	-local region	1.30 <sup>+0.17</sup> <sub>-0.14</sub>	0.43 <sup>+&gt;0.57</sup> <sub>-0.29</sub>	2.40 <sup>+0.23</sup> <sub>-0.42</sub>	0.58 <sup>+0.21</sup> <sub>-0.36</sub>	54.61599/50
South	blank-sky	1.44 <sup>+0.18</sup> <sub>-0.13</sub>	> 1.00 <sup>+&gt;0.0</sup> <sub>-0.62</sub>	2.21 <sup>+0.14</sup> <sub>-0.15</sub>	0.95 <sup>+0.11</sup> <sub>-0.25</sub>	74.33978/71
	model-bkg	1.40 <sup>+0.18</sup> <sub>-0.14</sub>	> 1.00 <sup>+&gt;0.0</sup> <sub>-0.62</sub>	2.14 <sup>+0.16</sup> <sub>-0.17</sub>	0.91 <sup>+0.13</sup> <sub>-0.27</sub>	77.66279/70
	model-bkg(Frzn)	1.44 <sup>+0.20</sup> <sub>-0.15</sub>	0.49 <sup>+&gt;0.51</sup> <sub>-0.32</sub>	2.33 <sup>+0.33</sup> <sub>-0.51</sub>	0.59 <sup>+0.26</sup> <sub>-0.42</sub>	90.72980/71
	-local region	1.43 <sup>+0.19</sup> <sub>-0.14</sub>	> 1.00 <sup>+&gt;0.0</sup> <sub>-0.76</sub>	2.27 <sup>+0.18</sup> <sub>-0.38</sub>	0.78 <sup>+0.11</sup> <sub>-0.46</sub>	76.28895/71

dersubtracted particle background, we repeated our four different techniques for handling the background that we had done for a single thermal model. As in the case with the single thermal model, the results are consistent within 90% for all the background techniques used (see Table 2). Also, we point out that the lack of a NT detection in the Western and Eastern regions provides more evidence that the detection in the Northern and Southern regions is not simply particle background, since that would be observed isotropically across the detector.

#### 4. Discussion

Comparing our results with the simulations done by Miniati et al. (2001), we argue that the localized diffuse NT emission is from a population of primary electrons. Miniati et al. (2001) find that primary electron reacceleration follows the shock region closely, with a spectral index of  $\alpha_{ic} \sim 1.1$  and increasing with distance from the shock. Our 90% confidence photon index  $\Gamma_X = 2.07\text{--}2.36$  which corresponds to a spectral index  $\alpha_{ic} = 1.07\text{--}1.36$  is consistent with the spectral index that Miniati et al.

(2001) found for primary electrons near a shock,  $\alpha_{ic} = 1.1$ , and steeper than the spectral index they found for secondary electrons,  $\alpha_{ic} < 1.1$ . Using the best fit  $F_{ic} - T_x$  of Miniati et al. (2001), we find a flux of  $(10-48) \times 10^{-13}$  ergs  $\text{cm}^{-2} \text{s}^{-1}$  over 0.13 to 100 keV for primary electrons in a 1.94 keV cluster (IC1262's temperature as determined by Hudson et al. (2003)). The range of fluxes depends on the  $R_{e/p}$ , the ratio of electrons to protons at relativistic energies. Using the same energy range and cluster temperature we find that secondary electrons produce a flux of  $1.9 \times 10^{-13}$  ergs  $\text{cm}^{-2} \text{s}^{-1}$ . For our best fit

photon index  $\Gamma_X = 2.21$  and 90% confidence normalization range of  $7.0-11.1 \times 10^{-5}$  photons  $\text{cm}^{-2} \text{s}^{-1} \text{keV}^{-1}$  at 1 keV, we determine a flux of  $(6-10) \times 10^{-13}$  ergs  $\text{cm}^{-2} \text{s}^{-1}$  for the 0.13–100 keV range. This result has a lower limit  $3\times$  greater than the results predicted for flux from secondary electrons. Although the 90% upper confidence limit is barely consistent with the primary electron model (suggesting  $R_{e/p} \sim 0.01$ ), we point out that our region of detection is at the base of the S3 chip, so that more NT emission is possible below this region.

### References

- Blasi, P. 2001, *Astroparticle Physics*, 15, 223  
 Colles, M., Saglia, R., Burstein, D., Davies, R., McMahan Jr., R., & Wegner, G. 2001, *MNRAS*, 321, 277.  
 Ebeling, H., Edge, A.C., Böhringer, H., Allen, S.W., Crawford, C.S., Fabian, A.C., Voges, W., & Huchra, J.P. 1998, *MNRAS*, 301, 881.  
 Enßlin, T. 1999, in *Diffuse Thermal and Relativistic Plasma in Galaxy Clusters*, ed. H. Böhringer, L. Feretti, & P. Schuecker (Garching:MPI), 249.  
 Fabian, A. C., Sanders, J. S., Allen, S. W., Crawford, C. S., Iwasawa, K., Johnstone, R. M., Schmidt, R. W., & Taylor, G. B. 2003, *MNRAS* in press (astro-ph/0306036)  
 Heinz, S., Choi, Y.-Y., Reynolds, C. S., & Begelman, M. C. 2002, *ApJ*, 569, 79.  
 Hudson, D.S., Henriksen, M. J., & Colafrancesco, S. 2003, *ApJ*, 583, 706.  
 Markevitch et al. 2003, *ApJ*, 586, 19.  
 McNamara, B.R. et al. 2001, *ApJ*, 562 L149.  
 Miniati, F., Jones, T. W., Kang, H., & Ryu, D. 2001, *ApJ*, 562, 233.